

Accounts

Two-Dimensional Correlation Spectroscopy: Principle and Recent Theoretical Development

Yukihiro Ozaki,* Slobodan Šašiċ, Takeyuki Tanaka,# and Isao Noda†

Department of Chemistry, School of Science, Kwansei-Gakuin University, Nishinomiya 662-8501

† Miami Valley Laboratories, The Procter and Gamble Co., 8256 Union Center Boulevared, West Chester, OH 45069, USA

(Received July 24, 2000)

This review paper aims at examining the recent developments in optical two-dimensional (2D) correlation spectroscopy. Particular emphasis is put on progress in the theory and calculation methods in 2D correlation spectroscopy. A historical review of 2D correlation spectroscopy is described first, and the mathematical treatment of generalized 2D correlation spectroscopy is explained next. Then a recently proposed efficient route to calculating 2D correlation spectra is reviewed in detail. Examples of applications of 2D correlation spectroscopy are also reported. In the last part of this article, a new possibility of the generalized 2D correlation spectroscopy, sample–sample correlation spectroscopy, is to be discussed.

The idea that, by spreading spectral peaks over the second dimension, one can simplify the visualization of complex spectra consisting of many overlapped bands was born in NMR spectroscopy about 30 years ago.[1–4] Since that time two-dimensional (2D) spectroscopy has been dominated by NMR and other related resonance spectroscopy techniques. The basic concept of 2D infrared (IR) spectroscopy was proposed by Noda in 1986.[5–7] The conceptual influence of 2D NMR on the early stage of 2D IR correlation spectroscopy was significant. For example, the convenient representation techniques used in 2D NMR, such as contour map representation and spectral slices, were instantly adopted to 2D IR. However, the specific experimental procedure developed for 2D IR spectroscopy is significantly different from that employed in 2D NMR. The major obstacle is that vibrational relaxation rates (picosecond range) are many orders of magnitude faster than the typical spin relaxation rates (microsecond range or even longer) encountered in NMR. Thus, unlike the time-domain double Fourier transform (FT) methods based upon multiple-pulse excitation employed in 2D NMR,[1–4] a simple cross-correlation analysis was applied to sinusoidally varying dynamic IR signals to obtain a set of 2D IR correlation spectra.[5–7] 2D IR correlation spectroscopy has been especially successful in the studies of systems stimulated by a small-amplitude mechanical or electrical perturbation.[8–17] The technique was first applied to the analysis of a rheo-optical dynamic IR dichroism measurement of a polymer film perturbed with a small-amplitude oscillatory strain. Dynamic fluctuations of IR dichroism signals due to the submolecular-level reorientational responses of polymer chain segments were analyzed by a 2D correlation scheme. The same 2D correlation analysis was utilized to explore similar reorientational responses of liquid crystalline samples induced by the application of an electric field. One can find many examples of the applications of 2D IR correlation spectroscopy in the studies of polymers and liquid crystals.[8–17]

One of the major shortcomings of the above 2D correlation approach, however, is that the time-dependent behavior (i.e., waveform) of dynamic spectral intensity variations must be a simple sinusoid to effectively employ the original data analysis scheme.[5–7] To overcome this limitation Noda[18] designed a more generally applicable, yet reasonably simple mathematical formalism, which enables one to handle signals fluctuating as an arbitrary function of time or any other physical variables to calculate 2D correlation spectra. This development has made the 2D correlation approach a universal spectroscopic tool, suitable for a very wide range of applications. Noda[18] named this new spectroscopy as *generalized 2D correlation spectroscopy*.

In generalized 2D correlation spectroscopy,[18] perturbations of various physical origins such as thermal, optical, and mechanical perturbations and waveforms such as sinusoid, pulse, and ramp can be used to construct 2D correlation spectra. Moreover, generalized 2D correlation spectroscopy does not

Present address: Faculty of Agriculture, Kobe University.

constrict the field of application to any particular electromagnetic probes. Thus, further extension of newly developed generalized 2D correlation scheme to other areas of spectroscopy, such as near-infrared (NIR), Raman, and fluorescence spectroscopy is also quite straightforward.

The advantages of the generalized 2D correlation spectroscopy lie in the following points: i) Simplification of complex spectra consisting of many overlapped peak, and enhancement of spectral resolution by spreading peaks over the second dimension; ii) Establishment of unambiguous assignments through correlation analysis of bands selectively coupled by various interaction mechanisms; iii) Probing the specific order of the spectral intensity changes taking place during the measurement or the value of controlling the variable affecting the spectrum; iv) Investigations of correlation between bands in two different spectroscopies, for example, correlation between an IR band and a Raman band and that between an IR band and an NIR band (heterospectral correlation).

The purpose of this review is to introduce the principle and recent theoretical development in 2D correlation spectroscopy. Particular emphasis is put on vibrational spectroscopy, i.e., IR, NIR, and Raman spectroscopy.

1. Recent Trends in Generalized 2D Correlation Spectroscopy

Generalized 2D correlation spectroscopy has opened up the possibility of introducing the powerful and versatile capability of 2D correlation analysis to a much wider range of applications, including complex reaction kinetics, electrochemistry, and photochemistry.[18–21] This concept is so flexible and general that it is applicable to any spectroscopic study. Thus far, generalized 2D correlation spectroscopy has been applied to IR, NIR, Raman, ultraviolet-visible (UV-Vis), fluorescence, and circular dichroism (CD) spectroscopy. However, the applications of 2D correlation spectroscopy are not limited to optical spectroscopy.[19–21] It has been applied also to X-ray scattering and mass spectrometry. There is one interesting example that shows the versatility of generalized 2D correlation; the basic idea of 2D correlation is applied to an area completely outside of spectroscopic analysis, showcasing the key features of findings from statistical mechanical analysis of polymer chain dynamics.[21]

(1) External Perturbations. The generalized 2D correlation spectroscopy lifted the constraint of the excitation waveform that the original 2D correlation spectroscopy had.[18] Thanks to the generalized 2D correlation scheme, one can use numerous types of external perturbations and physical stimuli that can induce spectral variations. The perturbations utilized in the 2D correlation analysis may be classified into two types.[19–21] One type yields the spectral data set as a direct function of the perturbation variable itself and the second type gives them as a function of the secondary consequence caused by the perturbation, such as time-dependent progression of spectral variations caused by the application of a stimulus. Temperature, pressure, and concentration belong to the former type, while mechanical deformation, electric field, and chemical reactions belong to the latter type. Even spatial distributions, polarization angle, and excitation wavelength become useful perturbations for 2D correlation spectroscopy.

(2) 2D Heterospectral Correlation. One of the most attractive fields in 2D correlation spectroscopy may be heterospectral correlation.[18,20,22–27] The heterospectral correlation analysis provides rich insight and clarification into the vibrational spectra.[22–27] For example, the correlation between NIR and IR spectroscopy is very interesting because by correlating NIR bands with IR bands for which the band assignments are better established, one may be able to investigate the band assignments in the NIR region.

2D heterospectral correlation analysis has been studied extensively by several research groups.[22–27] Noda, et al.[22] reported 2D heterospectral IR-Raman correlation analysis of N-methylacetamide. Czarnecki, et al.[23] investigated 2D heterospectral IR-NIR correlation analysis of temperature-dependent spectral variations of Nylon 12. A 2D NIR-IR correlation study of CMP kinases was carried out by Schultz, et al.[24] and a 2D IR-Raman correlation study of β-lactoglobulin was reported by Jung, et al.[27]

2. Background

Figure 1 illustrates a general scheme for obtaining 2D correlation spectra.[18] When an arbitrary perturbation is applied to a system, various chemical constituents of the system are selectively excited. The excitation and subsequent relaxation process toward the equilibrium can be monitored with electromagnetic probes. The intensity changes, band shifs, and changes in band shapes are typical spectral variations observed under external perturbation. The monitored fluctuations of spectral signals are then transformed into 2D spectra by use of a correlation method. However, before the calculation of 2D correlation spectra, dynamic spectra must first be calculated.

(1) Dynamic Spectra.[18,28,29] For a spectral intensity variation $y(\nu,t)$ observed as a function of a spectral variable ν during an interval of some additional external variable t between $T_{\min}$ and $T_{\max}$, the *dynamic spectrum* $\tilde{y}(\nu,t)$ is defined as

$$\tilde{y}(\nu,t) = \begin{cases} y(\nu,t) - \bar{y}(\nu) & \text{for } T_{\min} \le t \le T_{\max} \\ 0 & \textit{otherwise.} \end{cases} \quad (1)$$

The external variable t will be referred to as *time* for convenience, although it can be any reasonable measure of a physical quantity, such as temperature, pressure, and concentration.[18,28,29] The *reference spectrum* $\bar{y}(\nu)$ may often be set to the *time-averaged* spectrum defined by

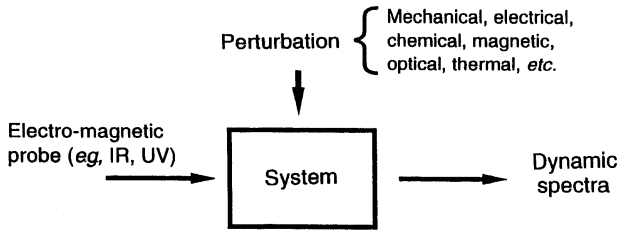

Fig. 1. General scheme for obtaining 2D correlation spectra.

$$\bar{y}(v) = \frac{1}{T_{\max} - T_{\min}} \int_{T_{\min}}^{T_{\max}} y(v,t)\mathrm{d}t \quad (2)$$

although other forms of reference spectra may also be chosen. It is essential for the mathematical consistency of the current analysis to explicitly set the value of $\tilde{y}(v,t)$ to be zero outside the boundary $T_{\max} \leq t \leq T_{\max}$.

Let us show one example of dynamic spectra. Figure 2(A) shows temperature-dependent FT-NIR spectra in the 9000–5000 cm^{-1} region of Nylon 12 obtained from 30 to 150 °C, and Fig. 2(B) displays dynamic NIR spectra corresponding to the temperature-dependent variations of the original FT-NIR spectra.[30] In this case, temperature was used as the external perturbation. Each dynamic spectrum can be regarded as a difference spectrum between the individual NIR spectrum and a preselected reference spectrum. In the present case, the reference spectrum was selected as the average of all spectral data. It can be seen from Fig. 2(B) that the dynamic spectra are powerful tools for monitoring the complex trends of thermally-induced intensity variations of NIR spectra of Nylon 12.[30]

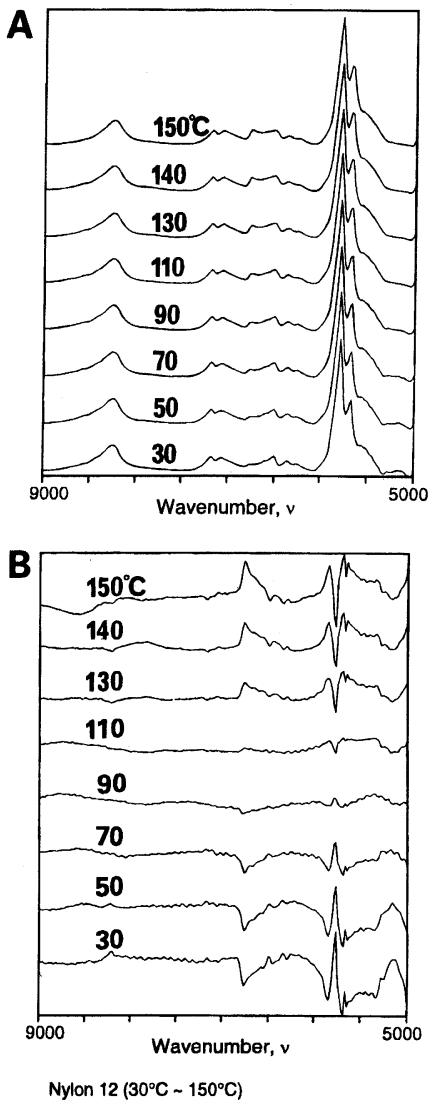

Fig. 2. (A) Temperature-dependent FT-NIR spectra in the 9000–5000 cm^{-1} region of Nylon 12 obtained from 30 to 150 °C. (b) Dynamic NIR spectra corresponding to the temperature-dependent variations of original FT-NIR spectra. (Reproduced from Ref. 30 with permission. Copyright (1997) American Chemical Societies).

(2) Generalized 2D Correlation Spectrum. A formal definition of the generalized 2D correlation spectrum is given by[18]

$$\Phi(\nu_1,\nu_2) + i\Psi(\nu_1,\nu_2) = \frac{1}{\pi(T_{\max} - T_{\min})} \int_0^{\infty} \tilde{Y}_1(\omega) \cdot \tilde{Y}_2^*(\omega)\mathrm{d}\omega \quad (3)$$

The *synchronous* and *asynchronous* 2D correlation spectrum, $\Phi(\nu_1,\nu_2)$ and $\Psi(\nu_1,\nu_2)$, represent, respectively, the overall similarities and differences of the time-dependent behavior of spectral intensity variations measured at two distinct spectral variables, ν_1 and ν_2, during the observation period between $T_{\min}$ and $T_{\max}$. The term $\tilde{Y}_1(\omega)$ is the forward Fourier transform of the spectral intensity variations $\tilde{y}(\nu_1,t)$ observed at some spectral variable ν_1

$$\begin{aligned}\tilde{Y}_1(\omega) &= \int_{-\infty}^{\infty} \tilde{y}(\nu_1,t)e^{-i\omega t}\mathrm{d}t \\ &= \tilde{Y}_1^{\mathrm{Re}}(\omega) + i\tilde{Y}_1^{\mathrm{Im}}(\omega)\end{aligned} \quad (4)$$

where $\tilde{Y}_1{}^{\mathrm{Re}}(\omega)$ and $\tilde{Y}_1{}^{\mathrm{Im}}(\omega)$ are, respectively, the real and the imaginary components of the Fourier transform. It is useful to remember that the real component $\tilde{Y}_1{}^{\mathrm{Re}}(\omega)$ is an even function of ω, while $\tilde{Y}_1{}^{\mathrm{Im}}(\omega)$ is an odd function. The Fourier frequency ω represents the individual frequency component of the variation of $\tilde{y}(\nu_1,t)$ measured along the variable t. Likewise, the conjugate of the Fourier transform $\tilde{Y}_2{}^*(\omega)$ of spectral intensity variations $\tilde{y}(\nu_2,t)$ observed at spectral variable ν_2 is given by

$$\begin{aligned}\tilde{Y}_2^*(\omega) &= \int_{-\infty}^{\infty} \tilde{y}(\nu_2,t)e^{+i\omega t}\mathrm{d}t \\ &= \tilde{Y}_2^{\mathrm{Re}}(\omega) - i\tilde{Y}_2^{\mathrm{Im}}(\omega).\end{aligned} \quad (5)$$

(3) Synchronous and Asynchronous Spectra. Figures 3A and 3B illustrate schematic counter maps of synchronous and asynchrounous spectra, respectively. The intensity of a synchronous 2D correlation spectrum represents the simultaneous or coincidental changes of spectral intensity changes measured at ν_1 and ν_2 during the interval between $T_{\min}$ and $T_{\max}$ of the externally defined variable t.[18] Autopeaks located at the diagonal positions represent the extent of dynamic variations of spectral intensity at different wavenumbers. Synchronous cross peaks appear at off-diagonal positions if the basic trends of dynamic variations observed at two different wavenumbers of the cross peak spectral coordinate are similar. Positive cross peaks indicate that intensities at both wavenumbers are either increasing or decreasing together, while negative peaks (usually marked by shading) show that one intensity is increasing and the other is decreasing.

An asynchronous 2D correlation spectrum $\Psi(\nu_1,\nu_2)$, which consists exclusively of off-diagonal cross peaks and is antisymmetric with respect to the diagonal line, provides information complementary to the synchronous spectrum.[18] The intensity of the asynchronous spectrum represents sequential or successive changes of spectral intensities measured at ν_1 and ν_2.

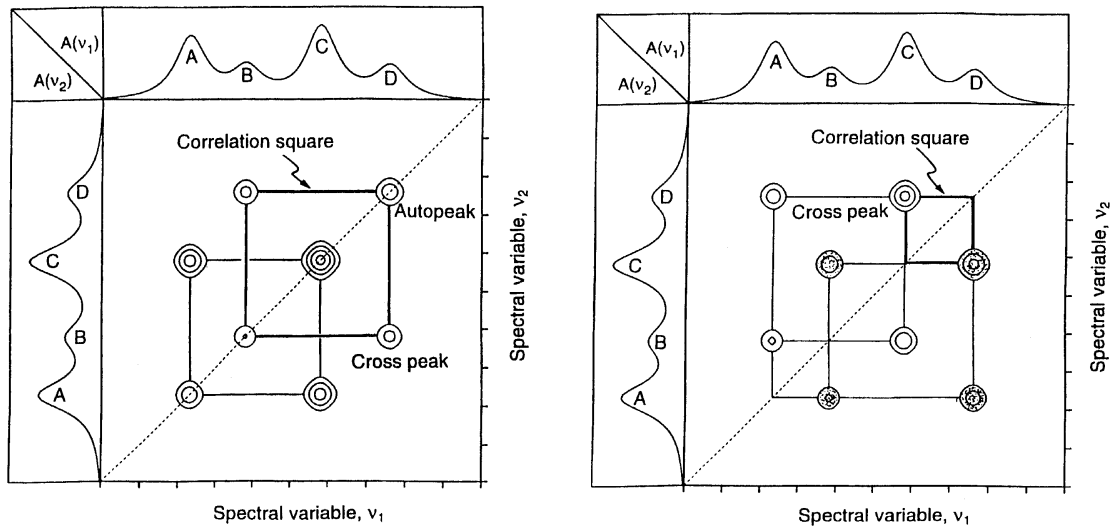

Fig. 3. (A) Schematic contour map of a synchronous 2D correlation spectrum. (B) Schematic contour map of an asynchronous 2D correlation spectrum.

Asynchronous cross peaks develop only if the basic trends of dynamic variations observed at two different wavenumbers of the cross peak spectral coordinate are dissimilar. This feature of asynchronous spectrum is especially useful in enhancing the spectral resolution of highly overlapped bands. By convention, a shaded asynchronous cross peak indicates that the event (increase of intensity) observed at wavenumber ν_1 occurs later compared to the event observed at wavenumber ν_2. The unshaded region of an asynchronous spectrum indicates the opposite.

While the formal definition of the 2D correlation intensities is mathematically rigorous, the computational steps involving the time-domain Fourier transformation of dynamic spectra are often cumbersome and time consuming. Thus, it is natural to explore an alternate and more efficient route to calculate 2D correlation spectra.

(4) More Efficient Route to Calculating 2D Correlation Spectra.[28,29] The basic concept of 2D correlation spectroscopy overlaps substantially the statistical cross-correlation analysis.[18,28,29] According to the classical time-series analysis,[31,32] the *cross-correlation function* between distinct dynamic spectral intensity variations observed at ν_1 and ν_2 for a fixed period of t between $T_{\min}$ and $T_{\max}$ is given by

$$C(\tau) = \frac{1}{T_{\max} - T_{\min}} \int_{T_{\min}}^{T_{\max}} \tilde{y}(\nu_1, t) \cdot \tilde{y}(\nu_2, t + \tau) \mathrm{d}t \qquad (6)$$

where τ is the *correlation time*. By applying the well-known Wiener–Khintchine theorem[32] to the above equation, the Fourier transform of a cross-correlation function (i.e., *cross spectrum*) can be directly related to the time-domain Fourier transform of dynamic spectral intensity variations as:

$$C(\tau) = \frac{1}{2\pi(T_{\max} - T_{\min})} \int_{-\infty}^{\infty} \tilde{Y}_1^*(\omega) \cdot \tilde{Y}_2(\omega) e^{i\omega\tau} \mathrm{d}\omega. \qquad (7)$$

By setting the correlation time to $\tau = 0$, Eq. 7 reduces to

$$C(0) = \frac{1}{2\pi(T_{\max} - T_{\min})} \int_{-\infty}^{\infty} \tilde{Y}_1^*(\omega) \cdot \tilde{Y}_2(\omega) \mathrm{d}\omega. \qquad (8)$$

(a) Synchronous 2D Spectrum. The imaginary component of a cross spectrum must consist exclusively of an odd function, so that the integration over the symmetric range of ω from $-\infty$ to $+\infty$ leaves only the even function or real component

$$C(0) = \frac{1}{\pi(T_{\max} - T_{\min})} \mathrm{Re}\left\{ \int_0^{\infty} \tilde{Y}_1^*(\omega) \cdot \tilde{Y}_2(\omega) \mathrm{d}\omega \right\}$$
$$= \frac{1}{\pi(T_{\max} - T_{\min})} \mathrm{Re}\left\{ \int_0^{\infty} \tilde{Y}_1(\omega) \cdot \tilde{Y}_2^*(\omega) \mathrm{d}\omega \right\}. \qquad (9)$$

Here, one can substitute the Fourier transform product with its conjugate because both have an identical real component. According to Eq. 8, the above expression is equivalent to $\Phi(\nu_1,\nu_2)$. Therefore, even without Fourier transforming dynamic spectra, the synchronous 2D correlation spectrum can be directly computed from Eq. 6 at $\tau = 0$ as

$$\Phi(\nu_1, \nu_2) = \frac{1}{T_{\max} - T_{\min}} \int_{T_{\min}}^{T_{\max}} \tilde{y}(\nu_1, t) \cdot \tilde{y}(\nu_2, t) \mathrm{d}t \qquad (10)$$

This result shows that the synchronous 2D correlation intensity is nothing but the time average of the product of dynamic spectral intensity variations measured at two different spectral variables, ν_1 and ν_2. The above simple computation method for a synchronous correlation spectrum is essentially equivalent to the method proposed by Fransinski et al.[33] or Marcott et al.[34] to calculated 2D covariance maps and also is closely related to the evaluation method of 2D correlation coefficient spectra proposed by Barton et al.[35]

The utilization of a cross-correlation function of dynamic spectral intensity variations allows one to compute only a synchronous 2D correlation spectrum. The calculation of an asynchronous spectrum is more complicated. Noda[18] showed that

for most practical applications the use of a heuristic disrelation spectrum is an excellent substitution for an asynchronous spectrum. Burie[36] revealed a clear and easy numerical procedure and easy numerical procedure for the computation of 2D spectra. However, most efficient short cut for the calculation of asynchronous spectra is to use the discrete Hilbert trancform.[28,29]

(b) Asynchronous 2D Spectrum and Use of Hilbert Transform. For a given analytic function $g(t)$, the *Hilbert transform* $h(t)$ of the function is given by

$$h(t) \equiv \frac{1}{\pi} pv \int_{-\infty}^{\infty} \frac{g(t')}{t' - t} \mathrm{d}t'. \tag{11}$$

The integration symbol $pv\int$ denotes that the *Cauchy principal value* is taken, such that the singularity at the point where $t' = t$ is excluded from the integration. It is well known that the Hilbert transform operation is closely associated with the Kramers–Kronig analysis of various spectra which are coupled by the orthogonal dispersion relationship.[28,29]

It can be easily pointed out by observing Eq. 11 that the Hilbert transform $h(t)$ may be regarded as the convolution integral between the two functions, $g(t)$ and $1/t$. From the convolution theorem, the Fourier transform of the Hilbert transform $h(t)$ becomes proportional to the product of the Fourier transforms of $g(t)$ and $1/t$.[28,29]

$$\begin{aligned} H(\omega) &= \int_{-\infty}^{\infty} h(t) e^{-i\omega t} \mathrm{d}t \\ &= \frac{1}{\pi} \int_{-\infty}^{\infty} \frac{1}{t} e^{-i\omega t} \mathrm{d}t \cdot \int_{-\infty}^{\infty} g(t) e^{-i\omega t} \mathrm{d}t \end{aligned} \tag{12}$$

Thus, the Fourier transforms of functions $g(t)$ and $h(t)$ are related by

$$\begin{aligned} H(\omega) &= i\mathrm{sgn}(\omega) \cdot G(\omega) \\ &= \begin{cases} G^{\mathrm{Im}}(\omega) - iG^{\mathrm{Re}}(\omega) & \omega < 0 \\ 0 \quad if & \omega = 0 \\ -G^{\mathrm{Im}}(\omega) + iG^{\mathrm{Re}}(\omega) & \omega > 0 \end{cases} \end{aligned} \tag{13}$$

where $G^{\mathrm{Re}}(\omega)$ and $G^{\mathrm{Im}}(\omega)$ are the real and imaginary components of the Fourier transform of the function $g(t)$. The value of *signum function* $\mathrm{sgn}(\omega)$ becomes -1, 0, or $+1$, if ω is smaller than, equal to, or greater than 0, respectively.

The above result provides a simplified view of the Hilbert transform relationship. The Hilbert transformation of a function shifts the phase of each Fourier component of a function *forward* by $\pi/2$ if $\omega > 0$ and *backward* if $\omega < 0$. Thus, the functions $g(t)$ and $h(t)$ are *orthogonal* to each other, i.e.,

$$\int_{-\infty}^{\infty} g(t) \cdot h(t) \mathrm{d}t = 0. \tag{14}$$

(c) Orthogonal Correlation Function. Let the orthogonal spectrum $\tilde{z}(\nu_2, t)$ be the time-domain Hilbert transform of the dynamic spectrum $\tilde{y}(\nu_2, t)$.

$$\tilde{z}(\nu_2, t) = \frac{1}{\pi} pv \int_{-\infty}^{\infty} \frac{\tilde{y}(\nu_2, t')}{t' - t} \mathrm{d}t' \tag{15}$$

In other words, the orthogonal spectrum is a function where the *phase* of each Fourier component of the temporal variation of the dynamic spectrum is shifted by $\pm\pi/2$. The two-dimensional *orthogonal correlation function* between different spectral intensity variations observed at ν_1 and ν_2 for a period between $T_{\min}$ and $T_{\max}$ is given by

$$D(\tau) = \frac{1}{T_{\max} - T_{\min}} \int_{T_{\min}}^{T_{\max}} \tilde{y}(\nu_1, t) \cdot \tilde{z}(\nu_2, t + \tau) \mathrm{d}t \tag{16}$$

where τ is the correlation time. The orthogonal correlation function defined above is nothing but a cross-correlation function between the dynamic spectrum and the orthogonal spectrum. By applying the Wiener–Khintchine theorem, the orthogonal correlation function can be directly related to the Fourier transforms of the dynamic spectrum and orthogonal spectrum as

$$D(\tau) = \frac{1}{2\pi(T_{\max} - T_{\min})} \int_{-\infty}^{\infty} \tilde{Y}_1^*(\omega) \cdot \tilde{Z}_2(\omega) e^{i\omega\tau} \mathrm{d}\omega. \tag{17}$$

where $\tilde{Z}_2(\omega)$ is the Fourier transform of $\tilde{z}(\nu_2, t)$. By setting $\tau = 0$, and by using the relationship $\tilde{Z}_2(\omega) = i\ \mathrm{sgn}(\omega) \cdot \tilde{Y}_2(\omega)$ based on Eq. 13, the above equation reduces to

$$D(0) = \frac{i}{2\pi(T_{\max} - T_{\min})} \int_{-\infty}^{\infty} \mathrm{sgn}(\omega) \tilde{Y}_1^*(\omega) \cdot \tilde{Y}_2(\omega) \mathrm{d}\omega. \tag{18}$$

The integration over the symmetric range of ω from $-\infty$ to $+\infty$ leaves only the imaginary component of the cross spectrum, since the signum function is an odd function. The substitution of the Fourier transform product with its conjugate, which by definition is equivalent to the sign change in the imaginary component, cancels the negative sign arising from multiplying an imaginary number by i. According to Eq. 3, the above expression is equivalent to $\Psi(\nu_1, \nu_2)$. Thus, the asynchronous 2D correlation spectrum can be computed directly from the dynamic spectrum and the orthogonal spectrum.

$$\Psi(\nu_1, \nu_2) = \frac{1}{T_{\max} - T_{\min}} \int_{T_{\min}}^{T_{\max}} \tilde{y}(\nu_1, t) \cdot \tilde{z}(\nu_2, t) \mathrm{d}t \tag{19}$$

This result shows that the asynchronous correlation intensity is equivalent to the time average of the product of dynamic and orthogonal spectrum measured at two different spectral variables, ν_1 and ν_2. Note that the evaluation of Eq. 19, like that of Eq. 10, does not require the Fourier transformation of dynamic spectral data.

(5) Recent Mathematical Developments in 2D Correlation Spectroscopy in Relation to Statistical Concepts. The progress of 2D correlation spectroscopy has been strongly linked not only with the developments of experimental techniques and instrumentation but also with progress of mathematical treatments for better data manipulation.[37] There have recently been some notable developments in the mathematical treatments, especially those related to the statistical theory. The notion of correlation phase angle has also been introduced.[37] The significance of correlation phase angle between dynamic fluctuations of signals measured at two different spectral variables may be linked to more commonly known statistical concepts, such as coherence and correlation coefficient. Reference 37 discussed in more detail about the relation to the statistical concept.

3. Applications of Generalized 2D Correlation Spectroscopy

This article does not aim at reviewing extensive amount of applications of 2D correlation spectroscopy. Instead, we give an overview of its applications very briefly.[8–17,22–27,30,38–57] From the point of optical probes used for monitoring responses to external perturbation, the applications of 2D spectroscopy can be divided into 2D IR,[8–17,22,24,27,40–44,47–49,53,56] 2D NIR,[24–26,30,38,39,45,46,51,55] 2D Raman,[22,25–27,50] 2D UV-vis (ultraviolet-visible),[52] 2D fluorescence,[57] 2D mass,[54] and so on. From the point of perturbation, they are classified into temperature-, pressure-, time-, concentration-,... dependent 2D correlation analysis. There is almost no limitation perturbation utilized in 2D correlation spectroscopy.

The application of 2D correlation spectroscopy are also classified into several groups based upon the materials and molecules to which 2D correlation spectroscopy is applied. Nowadays, it is applied to basic molecules, polymers, liquid crystals, biological molecules, biomedical materials, agricultural products, and foods. Emerging applications of diverse 2D correlation spectroscopy methods are almost limitless.

In the article two representative examples of recent applications of 2D correlation spectroscopy are introduced. One is 2D polarized IR spectroscopy study of molecular structure and orientation of a ferroelectric liquid crystal with a naphthalene ring.[53] In this study, a polarization angle is used as external perturbation. Another is 2D correlation analysis of NIR spectra of milk.[51] From this study one can recognize that 2D correlation spectroscopy is useful even for spectral analysis of complicated raw materials such as milk.

(1) 2D Polarized IR Spectroscopy Study of Molecular Structure and Orientation of a Ferroelectric Liquid Crystal with a Naphthalene Ring. Ferroelectric liquid crystals (FLC's) have recently received keen interest as the most recent member of the family of ferroelectric materials because of their potential applications in high resolution, flat panel displays and optical processing devices. An FLC in the Sm-C^* phase placed inside a cell of a few micrometers thickness may interact with the cell windows and form two stables states called the surface-stabilized FLC. By reversing the polarity of the applied electric field, molecules can be switched back and forth from one state to the other state at a fast speed in the microsecond range.

Although the functions of FLCs have been investigated actively, the detailed mechanism of field-induced reorientation of different segments of FLCs is not yet fully elucidated due to the complexity of their structure. During the last decade, time-resolved FT-IR and polarized IR spectroscopy has been applied as powerful tools for investigating the dynamics of electric-field-induced switching of FLCs.[15,53] Polarized IR spectroscopy enables one to investigate molecular structure and alignment of FLCs, because it gives useful information about polarization angle dependence for each functional group. However, the analysis of the polarization angle dependences of IR band intensities is not always straightforward, partly because some bands may overlap each other and partly because some bands may show very similar polarization angle dependences. Nagasaki et al.[53] demonstrated the potential of 2D correlation spectroscopy in analyzing the polarization angle dependences.

Figure 4 illustrates the structure of a FLC with a naphthalene ring (FLC-1) and the phase transition temperatures of FLC-1.[53] FLC-1 has a bookshelf layer structure for a particular alignment of the film in the Sm-C^* phase. Figure 5 shows polarized IR spectra of FLC-1 at 60° in the parallel ($\omega = 15°$) and perpendicular ($\omega = -75°$) polarization geometries (the polarization angle ω is taken as zero when the polarization direction of the incident IR radiation coincides with the rubbing direction).[53] The direction of ω = 15° is that of molecular long axis under dc voltage of +40 V, and the direction of $\omega = -75°$ is perpendicular to that of ω = 15°. From these spectra, the dichroic ratio D for the absorption bands, defined as the ratio of the absorbances for the parallel and perpendicular polarizations of light, was calculated. The assignments and dichroic ratios for the isolated and relevant bands are listed in Table 1.[53]

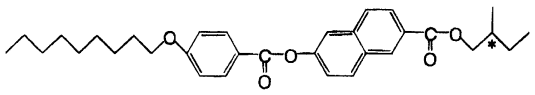

FLC-1

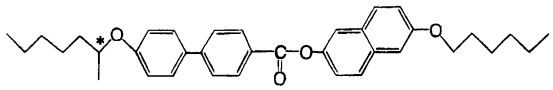

FLC-2

Fig. 4. Structure and phase transition sequence of FLC-1.

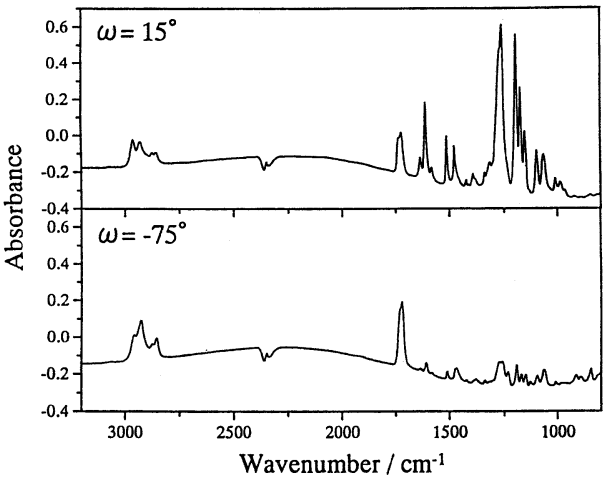

Fig. 5. Polarization IR spectra of FLC-1 at 60 °C in the parallel ($\omega = 15°$) and perpendicular ($\omega = -75°$) polarization geometries. (Reproduced from Ref. 53 with permission. Copyright (2000) American Chemical Societies).

Table 1. Dichroic Ratio (D) and Vibrational Band Assignments for the Relevant Peaks in the Infrared Spectra of FLC-1 in the Sm-C^* Phase (From Ref. 53)

Wavenumber / cm^{-1} a)	D ($A_{\parallel}/A_{\perp}$)	Assignment b)
2960(m)	0.8	CH_3 asym. st.
2928(s)	0.6	CH_2 antisym. st.
2874(m)	0.8	CH_3 sym. st.
2856(m)	0.5	CH_2 sym. st.
1736(s, sh)	0.8	C=O st. (core)
1721(s)	0.6	C=O st. (chiral)
1606(m)	9.5	ring C=C st.
1510(m)	6.8	ring C=C st.
1475(m)	3.2	
1274(m)	6.3	C–O–C antisym. st.
1257(m)	8.0	C–O–C antisym. st.
1192(m)	9.0	
1170(m)	9.8	ring CH def.
1150(m)	6.5	
1096(m)	5.8	C–O–C sym. st.
1065(m)	2.7	C–O–C sym. st.

a) w, weak ; m, medium ; s, strong ; sh, shoulder.
b) sym, symmetric ; asym, asymmetric ; antisym, antisymmtric ; st, stretching ; def, deformation.

Figure 6 illustrates normalized absorptivity (absorptivity = 1 – transmittance) versus polarization angle for the bands at 2928, 1736, 1721, 1606, 1192, 1170, and 1150 cm^{-1}.[53] To calculate the absorptivity of overlapped bands at 1736 and 1721 cm^{-1}, Nagasaki et al.[53] carried out curve fitting. It is noted that the two C=O stretching bands, particularly the band at 1736 cm^{-1}, show a polarization angle dependence clearly different from the other bands. The behavior of two C=O stretching bands is very important, because the carbonyl groups have large polarization, and thus are related to the ferroelectricity.

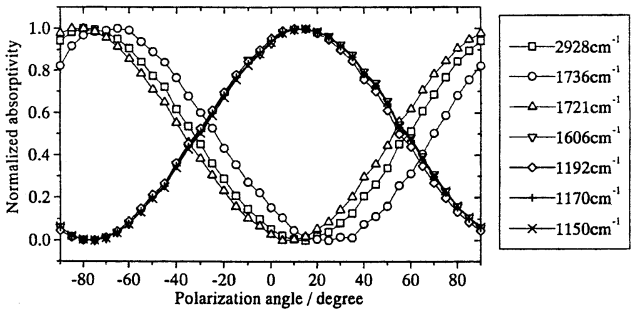

Fig. 6. Normalized absorptivity versus polarization angle for some representative bands in the polarized IR spectra of FLC-1 in the Sm-C^* monodomain at 60 °C under dc electric field of +40 V. (Reproduced from Ref. 53 with permission. Copyright (2000) American Chemical Societies).

The band due to the carbonyl group in the core part is observed at 1736 cm^{-1}, while that in the chiral part appears at 1721 cm^{-1}. For other bands, the band at 1606 cm^{-1} is attributed to the ring stretching mode, and that at 2926 cm^{-1} is assigned to CH_2 antisymmetric stretching mode. The phases in the intensity changes of three bands at 1606, 1192, 1170, and 1150 cm^{-1} are almost the same, and the change in the band at 2926 cm^{-1} is antiphase to them. However, the phase in the changes of the two carbonyl bands is different from those of other bands (Fig. 6). This indicates the hindered rotation around the molecular long axis of the carbonyl groups. Since each carbonyl group is attached to the benzene and naphthalene rings separately, there may be significant effects of the hindered rotations of the two carbonyl groups on the behavior of the two aromatic rings. The 2D correlation analysis gives a clear answer for this. Figure 7 shows (A) synchronous and (B) asynchronous 2D correlation

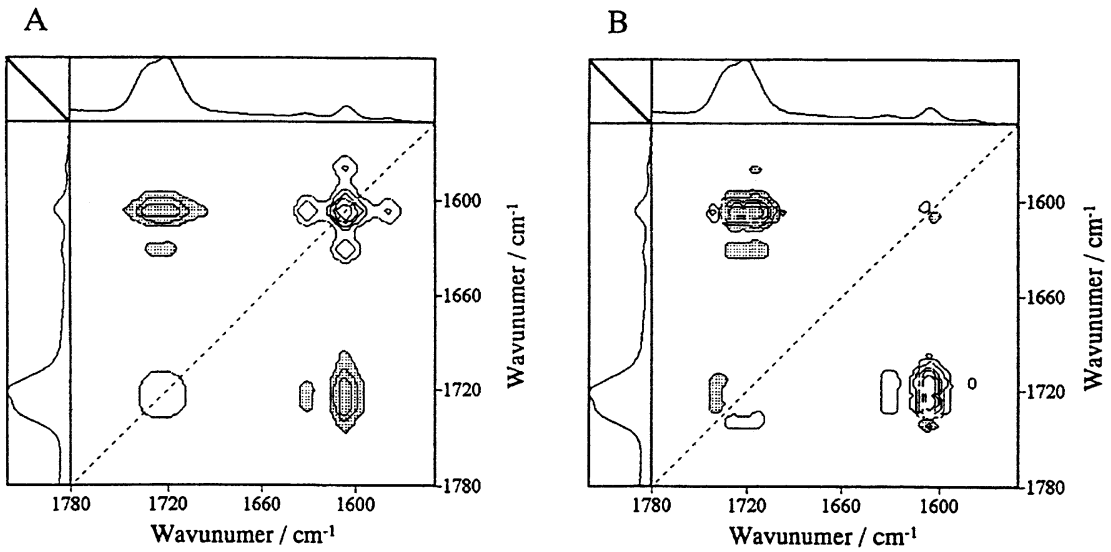

Fig. 7. (A) Synchronous and (B) asynchronous 2D infrared correlation spectra in the 1780–1550 cm^{-1} region generated from the polarization angle (between −90° and 90°)-dependent polarized spectral variations of FLC-1 in the Sm-C^* momodomain at 60 °C under dc electric field of +40 V. (Reproduced from Ref. 53 with permission. Copyright (2000) American Chemical Societies).

spectra in the 1780–1550 cm^{-1} region, generated from the polarization angle dependent IR spectra of FLC-1.[53] Note that one strong auto peak is clearly observed at 1606 cm^{-1}. This peak corresponds to the stretching modes of the benzene and naphthalene rings. This suggests that the intensity of the band due to the ring stretching modes changes significantly with the polarization angle. There are negative cross peaks at (1736, 1606) and (1721, 1606) cm^{-1}, indicating that the two C=O stretching bands and the ring stretching band show the polarization angle dependent intensity changes in the reverse direction.

The asynchronous spectrum developed three cross peaks at (1608, 1736), (1608, 1728), and (1608, 1715) cm^{-1}. This is clear evidence for the existence of three C=O stretching bands. The splitting of the band near 1721 cm^{-1} due to the chiral carbonyl group may be ascribed to the rotational isomerism around the O–C bond; there may be two conformers around the O–C bond. The signs of the cross peaks indicate that the phase of the intensity change in lower frequency components of the two C=O stretching bands is delayed compared with that of the high-frequency component. Moreover, the signs of cross peaks between the C=O stretching bands and the ring stretching band suggest that as the polarization angle is changed, the band intensity is varied in the order of bands at 1736, 1606, and 1728 and 1715 cm^{-1}. This conclusion is consistent with the observation in Fig. 6. Another notable observation in the asynchronyous spectrum is appearance of cross peaks near 1600 cm^{-1}. It is very likely that the ring stretching bands of the benzene and naphthalene rings appear separately in the cross peaks. The existence of the cross peaks in the asynchronous spectrum suggests that the directions of the transition moments of the ring stretching modes of the two aromatic rings are different and that the rotations of the two rings are hindered.

Figures 8A and B depict synchronous and asynchronous 2D IR correlation spectra between the 1780–1550 and 3000–2800 cm^{-1} regions generated from the polarization angle (between –90° and +90°)-dependent polarized spectral variations of FLC-1 in the Sm-C^* monodomain at 60 °C under dc electric field of +40 V.[53] The asynchronous spectrum in Fig. 8B reveals that the band at 2945 cm^{-1} has a positive cross peak with the band at 1606 cm^{-1}, while the band at 2965 cm^{-1} shares a negative cross peak with the same band. The original spectra show only one band due to the asymmetric CH_3 stretching mode at 2960 cm^{-1}. Probably, both bands at 2965 and 2945 cm^{-1} are due to the asymmetric CH_3 stretching modes of different CH_3 groups of FLC-1 whose intensities show different polarization angle dependences. The two CH_3 bands at 2965 and 2945 cm^{-1} show different signs in the cross peaks at (2965, 1606) and (2945, 1606) cm^{-1}, suggesting that the two bands have completely different polarization angle dependences. The band at 2945 cm^{-1} may be due to the chiral CH_3 groups because it is likely that only this band, whose transition moment is in the direction of the short molecular axis, appears separately. This study demonstrated the potential of 2D correlation spectroscopy in detection of slight differences in the polarization angle dependent intensity variations. A new possibility of 2D correlation spectroscopy in LC research was elucidated.

(2) 2D Correlation Analysis of NIR Spectra of Milk; Protein and Fat Concentration-Dependent Spectral Changes of Milk. Czarnick-Matusewicz, et al.[51] demonstrated the potential of generalized 2D correlation spectroscopy in analyzing NIR spectra of milk, a complicated biological fluid consisting mainly of proteins, fats, and carbohydrates. The signal-to-noise ratio of NIR spectra of milk is rather poor and their baselines change from one spectrum to another. Thus, the NIR spectra of 165 milk samples with different protein and fat concentrations were subjected to multiplicative scatter correction (MSC) and the smoothing, and the synchronous and asynchronous spectra were generated for protein or fat concentration-

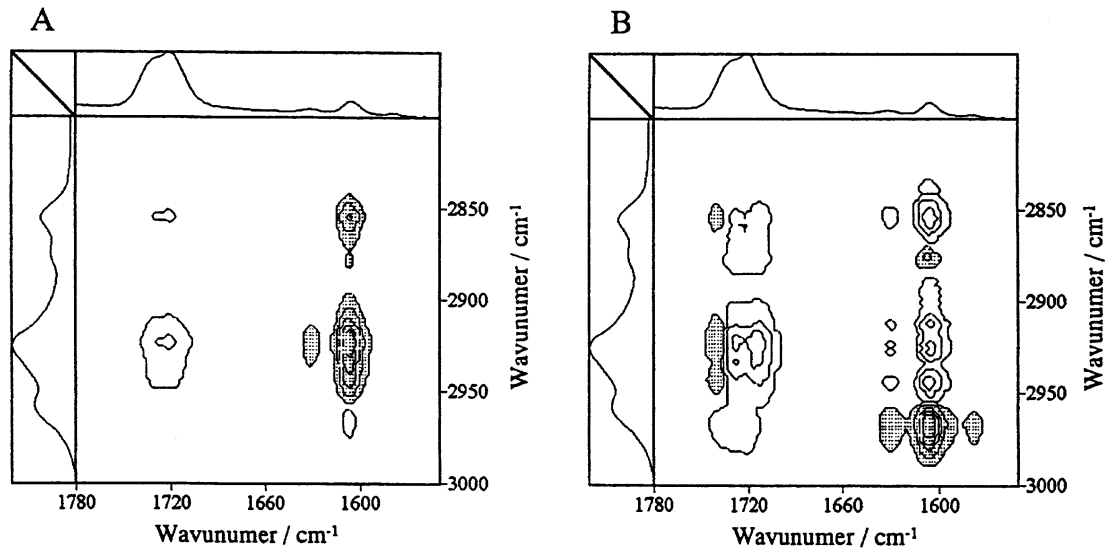

Fig. 8. (A) Synchronous and (B) asynchronous 2D infrared correlation spectra between the 1780–1550 cm^{-1} and 3000–2800 cm^{-1} regions generated from the polarization angle (between −90° and 90°)-dependent polarized spectra variations of FLC-1 in the Sm-C^* monodomain at 60 °C under dc electric field of +40 V. (Reproduced from Ref. 53 with permission. Copyright (2000) American Chemical Societies).

dependent spectral changes of milk.

Figure 9 displays together NIR spectra of the 165 milk samples.[51] A broad band near 1450 nm is due to the combination of OH symmetric and antisymmetric stretching modes of water, while an intense feature near 1930 nm is assigned to the combination of OH bending and symmetric stretching modes of water. The water bands are so strong that it is almost impossible to extract information about fats, proteins, lactose and other metabolites of milk directly from the NIR spectra.

Czarnick-Matusewicz, et al.[51] applied 2D correlation analysis to the NIR spectra of milk after MSC and smoothing. For the MSC treatment, two data segments were constructed, one from 1100 to 1900 nm and another from 2000 to 2400 nm. Figures 10A and B depict synchronous 2D correlation spectra in the 2000–2400 nm region generated from the fat or protein concentration-dependent NIR spectral changes after the pretreatments, respectively.[51] The synchronous spectrum constructed from the fat concentration-dependent NIR spectral changes develops autopeaks at 2311 and 2346 nm, while the corresponding spectrum from the protein concentration-dependent variations shows autopeaks at 2047, 2075, 2100, 2351, and 2375 nm. The appearances of the autopeaks mean that the intensities of these bands vary most significantly with increasing the concentrations of fats or proteins in milk.

Figures 11A and B present power spectra along the diagonal line on the synchronous spectra shown in Figs. 10A and B, respectively.[51] Of particular note in the power spectra is that most of the peaks which appear in the power spectrum for the fat concentration-dependent spectral variations (Fig. 11A) correspond to the bands due to fats while those in the power spectrum for the protein concentration-dependent spectral variations (Fig. 11B) are ascribed to proteins. Therefore, generalized 2D correlation spectroscopy can select out the bands due to fats and proteins separately from the complicated NIR spectra of milk.

Figure 12A depicts an asynchronous 2D NIR correlation map generated from fat concentration-dependent spectral variations of milk. The asynchronous map shows a number of peaks. Figure 12B shows a slice spectrum at 2311 nm, a characteristic wavelength for fat species.[51] Peaks are observed at 2054, 2066, 2318, 2334, 2354, and 2366 nm in the slice spectrum. The peaks at 2054, 2066, 2318, 2334, and 2366 nm are missing in the corresponding synchronous spectrum shown in Fig. 10A. In general, asynchronous correlation spectra have more powerful deconvolution ability for highly overlapped bands. Assignment of the bands observed in the 2000–2400 nm region of the NIR spectra of milk is summarized in Table 2.[51]

Figures 13A and B show synchronous 2D correlation spectra in the 1100–1900 nm region constructed from the fat and protein concentration-dependent spectral variations, respectively.[51] These two synchronous spectra show marked differences in the 1400–1500 nm region where bands due to the combination modes of various species of water are expected to appear. Proteins are hydrophilic while fats are hydrophobic, so that the protein–water interaction and the fat-water interaction are quite different from each other, giving large spectral differences in the 1400–1500 nm region. It is noted that the bands in the 1400–1500 nm region are separated into two in the synchronous spectrum for the protein concentration-dependent spectral variations (Fig. 13B). It is very likely that the two autopeaks at 1419 and 1485 nm in the synchronous spectrum in Fig. 13B arise from bulk and hydrated water, respectively. The assignments of the bands in the 1100–1900 nm region are also tabulated in Table 2.[51] This study is a good example showing that 2D correlation spectroscopy is useful even for spectral analysis of real world materials that yield rather poor signal-to

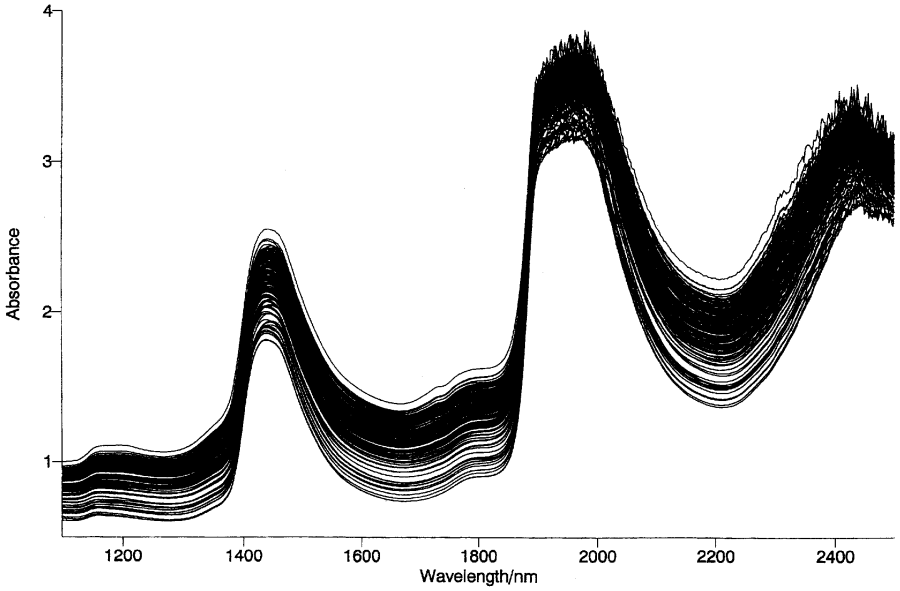

Fig. 9. NIR spectra in the 1100–2500 nm region of the milk samples (Reproduced from Ref. 51 with permission. Copyright (1999) Society for Applied Spectroscopy).

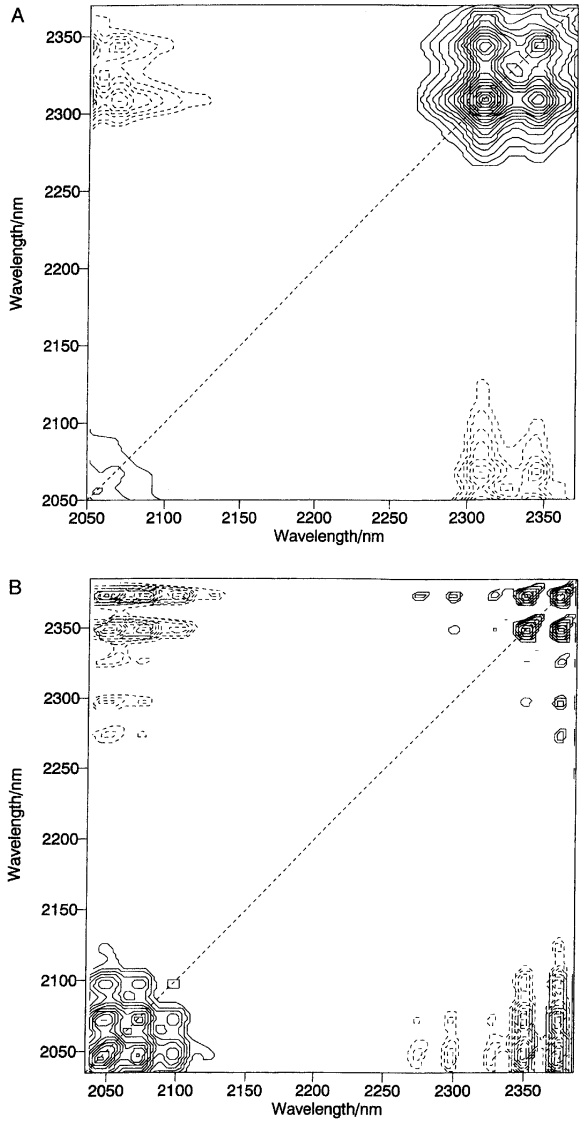

Fig. 10. Synchronous 2D NIR correlation spectra in the 2000–2400 nm region constructed from fat (A) and protein (B) concentration-dependent spectral changes of milk after MSC and smoothing. (Reproduced from Ref. 51 with permission. Copyright (1999) Society for Applied Spectroscopy).

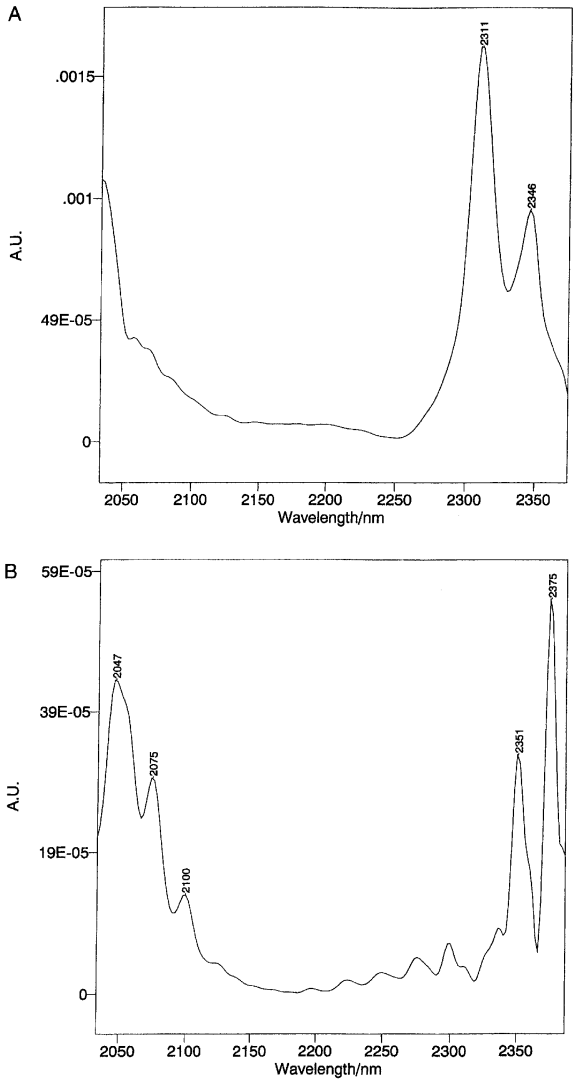

Fig. 11. (A) A power spectrum along the diagonal line on the synchronous spectrum shown in Fig. 2(A). (B) A power spectrum along the diagonal line on the synchronous spectrum shown in Fig. 2(B). (Reproduced from Ref. 51 with permission. Copyright (1999) Society for Applied Spectroscopy).

noise ratios and baseline changes.

4. Representations of Synchronous and Asynchronous Correlation Spectra by Linear Algebra

Recently, Šašič, et al.[58,60] have shown that synchronous and asynchronous correlation spectra can be represented by linear algebra. They considered the experimental matrix from the view of the conceptions of 2D correlation spectroscopy. In general, an experimental matrix **M** has dimensions of w x s, where w is the number of wavenumbers and s is that of samples. Every row of the data matrix can be viewed as a vector of the spectral intensity changes at a given wavenumber. Thus, one has a total of w such vectors with s coordinates. If one wants to compare these vectors, i.e., to find what the relation is between the intensity changes for any particular pair of wavenumbers v_1 and v_2, then one should multiply **M** by $\mathbf{M}^{\mathbf{T}}$ and form so-called rows cross product matrix **Z** (covariance matrix). **Z** is a square matrix of $w \times w$

$$\mathbf{Z} = 1/(s-1)\mathbf{M}\mathbf{M}^{\mathbf{T}}. \tag{20}$$

Any element of **Z** can be expressed as

$$Z_{ij} = 1/(s-1)\sum_{k=1}^{s} M_{ik}M_{kj}^{T}. \tag{21}$$

Elements of **Z** show similarity or dissimilarity between intensity variations for a pair of wavenumbers v_1 and v_2. **Z** is symmetric with respect to the diagonal line on which are placed auto-

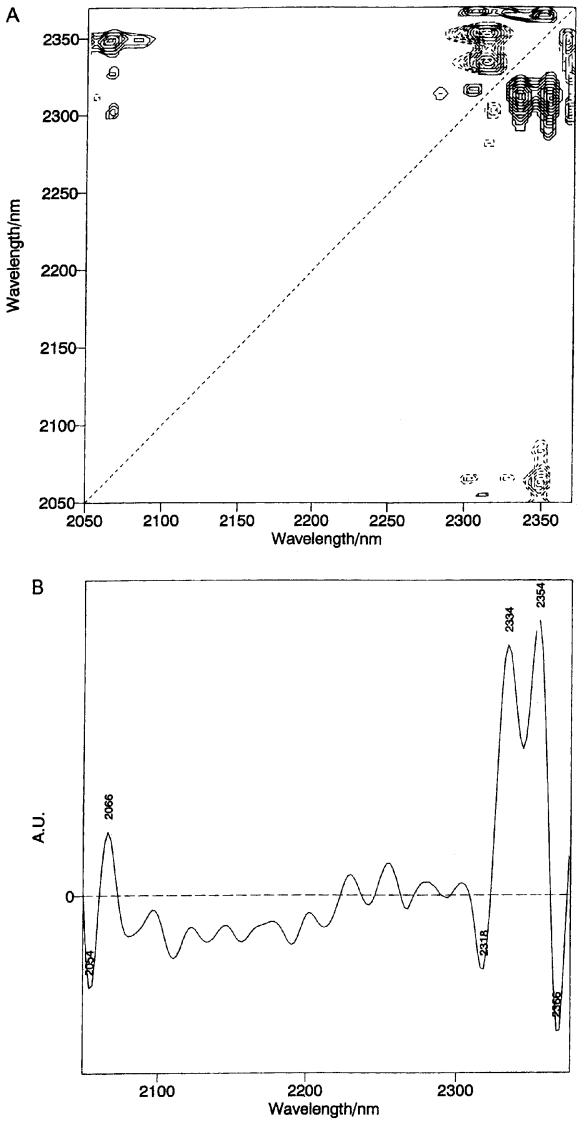

Fig. 12. (A) An asynchronous 2D NIR correlation spectrum in the 2000–2400 nm region constructed from fat concentration-dependent spectral changes of milk after the pretreatments. (B) A slice spectrum along 2311 nm line in the asynchronous spectrum shown in Fig. 4 (A). (Reproduced from Ref. 51 with permission. Copyright (1999) Society for Applied Spectroscopy).

correlation (v_i versus v_i) data. It is noted that **Z** holds all the features of the synchronous spectrum, and in fact it is a synchronous spectrum obtained by generalized 2D correlation spectroscopy. It is very important to recognize the relation between the synchronous spectrum and the cross product matrix because the latter is a well-known conception in the field of classic correlation analysis. Therefore, the synchronous spectrum can be considered as a table of the correlation coefficients between dynamics vectors of a given spectral matrix.

Equation 21 reveals that the asynchronous spectrum may also be expressed by a kind of rows cross product matrix. This time, however, it is not a correlation between dynamic vectors

Table 2. Proposed Assignment of Bands Observed in the 2D Synchronous and Asynchronous Spectra of Milk (From Ref. 51)

Band position/nm	Assignment
2382–2366	$\nu_s(CH_2) + \nu_s(CH_2)$–*psch*
2355–2351	$\nu_s(CH_3) + \nu_s(CH_3)$–*psch*
2346–2345	$\nu_s(CH_2) + \nu_s(CH_2)$–*fcch*
2335–2332	$\nu_s(CH_2) + \nu_a(CH_2)$–*psch*
2318	$\nu_a(CH_2) + \nu_a(CH_2)$–*psch*
2308–2311	$\nu_s(CH) + \nu_s(CH)$–*fcch*
2186	amide A + amide III
2160	amide B + amide II
2124	amide B + amide I
2100	amide B + amide I
2075–2038	amide A + amide I
1762–1761	first overtone of $\nu_s(CH_2)$–*fcch*
1728	first overtone of $\nu_a(CH_2)$–*fcch*
1638	first overtone of amide B
1584	first overtone of amide A
1468–1448	$\nu_s(OH) + c_a(OH)$ - hydrated water
1414–1390	$\nu_s(OH) + \nu_a(OH)$ - bulk water
1255–1250	first overtone of amide A + amide II

psch- protein side chains; *fcch*- fat hydrocarbon chain.

of the experimental matrix but one between these vectors and dynamic vectors of Hilbert orthogonalized $\mathbf{M}^{\mathbf{T}}$. The matrix orthogonalized to $\mathbf{M}^{\mathbf{T}}$ is denoted by **R**. Every element of **R** can be expressed as

$$R_{ij} = \sum_{k=1}^{s} H_{ik} M_{kj}^{T}. \quad (22)$$

The idea that synchronous and asynchronous spectra can be expressed as a rows cross product of the experimental matrix and a product of the experimental matrix and the orthogonalized or transposed matrix, respectively, led Šašič, et al.[58,59] to propose an extension of the generalized 2D correlation spectroscopy, sample–sample correlation spectroscopy as will be described later.

5. Sample–Sample Correlation Spectroscopy

Recently, Šašič, et al.[58,59] have proposed a new possibility of the generalized 2D correlation spectroscopy. Instead of generating 2D maps with the wavenumber axes and discussing correlations between bands, it is possible to create totally new generalized 2D correlation maps having sample axes, which was named the sample–sample correlation.[58,59] By use of this novel correlation method, one can discuss the concentration dynamics directly. By analogy to the existing generalized 2D correlation analyses that allows one to set spectral variables of any kinds of spectroscopy in wavenumber axes, the newly proposed sample–sample correlation can set any kind of perturbation variables, such as temperature, concentration, pressure and time, in sample axes. One may obtain temperature-temperature correlation spectroscopy, concentration-concentration correlation spectroscopy and so on, depending upon the perturbation.

(1) Principle of Sample–Sample Correlation Spectrosco-

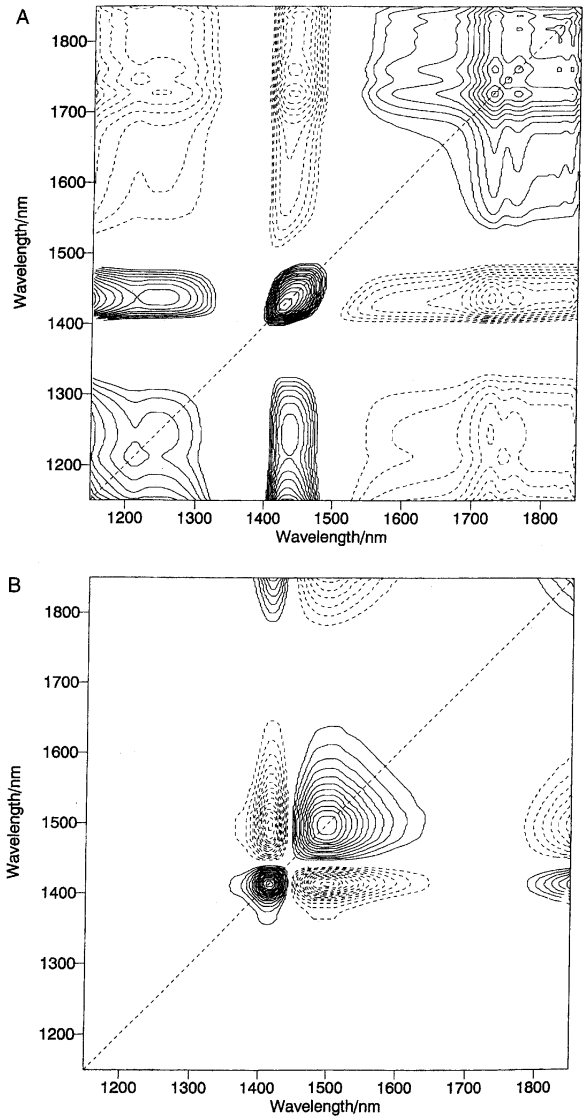

Fig. 13. Synchronous 2D NIR correlation spectra in the 1100–1900 nm region constructed from fat (A) and protein (B) concentration-dependent spectral changes of milk after the pretreatments. (Reproduced from Ref. 51 with permission. Copyright (1999) Society for Applied Spectroscopy).

py. The experimental matrix **M** can be viewed as a product

$$\mathbf{M} = \mathbf{WS} \tag{23}$$

where $\mathbf{W}(w \times n)$ is a matrix of the n pure spectrum (w points) and $\mathbf{S}$ $(n \times s)$ is a matrix of the n concentration profiles (s points). The synchronous spectrum represents relations between columns of **W**, i.e., between pure component spectra. In general, the axes of the generalized 2D correlation spectra denote wavenumbers, wavelength, or frequency. However, as one can see from Eq. 23, the experimental matrix contains information about the concentrations. Thus, the covariance matrix **Z** shows a correlation between concentrations by the following equation as in the case of the wavenumber-wavenumber correlation:

$$\mathbf{Z} = 1/(w-1)\mathbf{M}^{\mathbf{T}}\mathbf{M} \tag{24}$$

If we refer to principal component analysis (PCA), we shall see that two types of the covariance matrices can be formed.[58] The matrix calculated by Eq. 20 is the spectral cross-product matrix and by its decomposition it is possible to obtain information about the spectral features of components of samples (loadings), while the cross-product matrix obtained by Eq. 24 provides nowledge about concentration dynamics of components (scores). Both matrices show the different aspects of the species, spectra and concentrations examined.

The cross-product matrix formed by Eq. 24 yields a 2D correlation spectrum with the samples on both axes, and each point in the 2D map represents a correlation between the concentrations of a given pair of samples, s_i and s_j. The orthogonal cross correlation, or asynchronous sample–sample correlation spectrum can also be calculated after the orthogonalization rows of $\mathbf{M}^{\mathbf{T}}$. In this concept, the spectra are considered as the intensity changes with the samples while ordinary spectra are supposed to be spectral responses. The sample–sample correlation spectroscopy offers the possibility for fast analysis of the concentration changes of the species as a function of temperature, pressure, time, etc. The results obtained from this method can be easily combined with those from the wavenumber-wavenumber correlation analyses. These results make an entirety together because they depict two essential qualities of any spectral system: the amount of the species present and their own spectra.

(2) Application of Sample–Sample Correlation Spectroscopy. As an example of the application of sample–sample correlation spectroscopy, temperature-dependent NIR spectral variations of oleic acid (*cis*-9-octadecenoic acid) in the pure liquid state were analyzed in the region of 7600–6600 cm^{-1}.[60] Iwahashi et al.[61,62] showed, based upon a number of spectroscopic and physicochemical studies, that oleic acid has three kinds of liquid structures depending on temperature. In the temperature range from the melting point (15 °C) to 30 °C, the liquid structure consists of clusters having a quasi-smectic liquid crystal structure. The structure in the temperature range between 30 and 55 °C is composed of clusters with a less ordered structure. Above 55 °C oleic acid appears to be an isotropic liquid. NIR spectroscopy provided important evidence for the phase transitions of oleic acid in the pure liquid state.[62] Figure 14 shows NIR spectra in the 7600–6600 cm^{-1} region of oleic acid in the pure liquid state over a temperature range of 15–80 °C. Bands at 7194, 7092, and 6993 cm^{-1} are assigned to combination modes of the CH vibrations.[62] The peak heights of these bands gradually decrease with temperature due to the decrease in the density of the acid. A band at 6917 cm^{-1} consists of two components bands: one is due to a combination mode of the CH vibrations and another arises from the first overtone of the OH stretching vibration of the monomer. The intensity of this band increases as a function of temperature, giving good evidence that the acid dimer dissociates into the monomeric species even in the pure liquid state.[62] On the lower wavenumber side of the spectra in Fig. 14 appears the strong influence of a

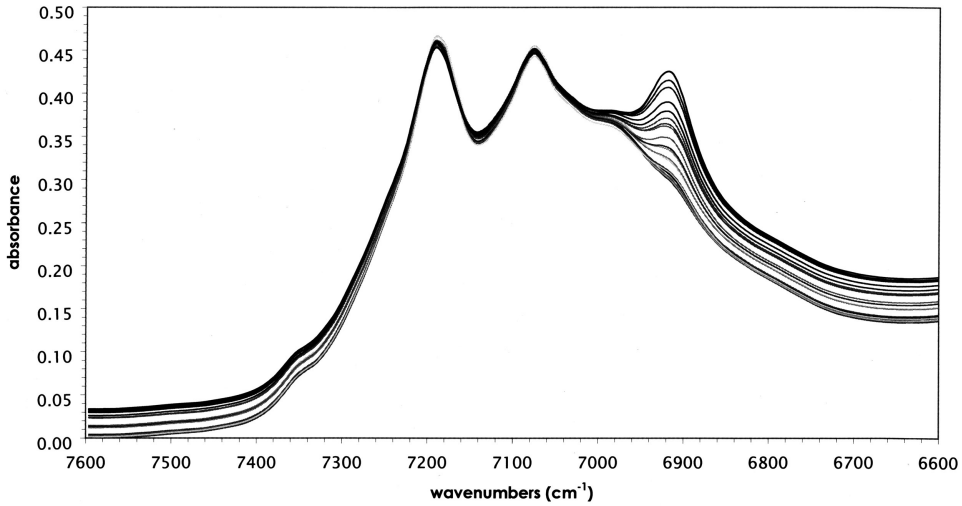

Fig. 14. NIR spectra in the 7600–6600 cm^{-1} region of oleic acid in the pure liquid state over a temperature range of 15–80 °C. (Reproduced from Ref. 59 with permission. Copyright (2000) American Chemical Societies).

broad band due to the hydrogen bonded O–H group of dimers located around 5850 cm^{-1}. On the higher wavenumber side, the baseline increases with temperature as a consequence of the change in the density of the sample. Šašič, et al.[59] applied both the wavenumber–wavenumber correlation and sample–sample correlation analysis to the set of spectra in Fig. 14.

Figures 15A and B show the synchronous and asynchronous wavenumber–wavenumber correlation maps calculated from the spectra shown in Fig. 14, respectively. The synchronous spectrum shows strong autopeaks at 7189 and 7076 cm^{-1}, and these peaks have negative correlation with the band at 6917 cm^{-1} and with the region of 7600–7300 cm^{-1}. The influence of the density change is very notable in the synchronous spectrum. The asynchronous spectrum yields information mostly about the relations between the monomer band at 6917 cm^{-1} and other spectral features. There is a positive correlation between the band at 6917 cm^{-1} and the whole region of 7600–7300 cm^{-1} and there are negative correlations at (6917,7186) and (6917,7080) cm^{-1}. These observations suggest that the band at 6917 cm^{-1} changes quite differently with temperature from the C–H bands and those in the region of 7600–7300 cm^{-1}.

Figures 16A and B illustrate a synchronous sample–sample correlation spectrum generated from the spectra in Fig. 14 and its slice spectra, respectively.[59] One can see that the slice spectra provide undoubted evidence for the two break points at 32 and 55 °C. It can be seen from the correlation patterns in Figs. 15 and 16 that the spectra without any baseline correction em-

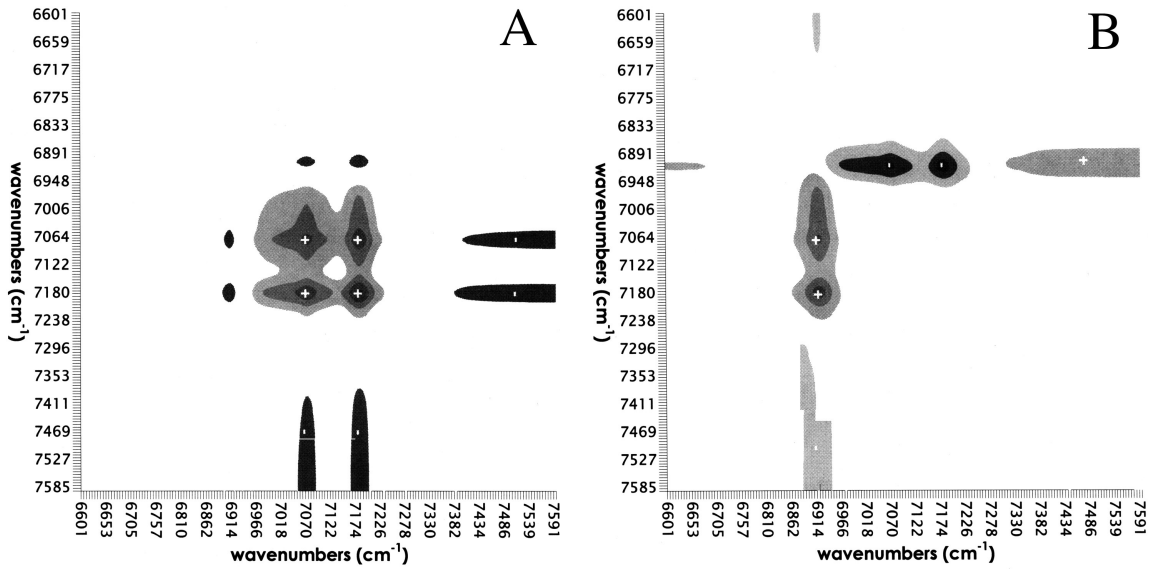

Fig. 15. (A) A synchronous spectrum of the wavenumber-wavenumber correlatioon calculated from the spectra shown in Fig. 14. (B) The corresponding asynchronous spectrum. (Reproduced from Ref. 59 with permission. Copyright (2000) American Chemical Societies).

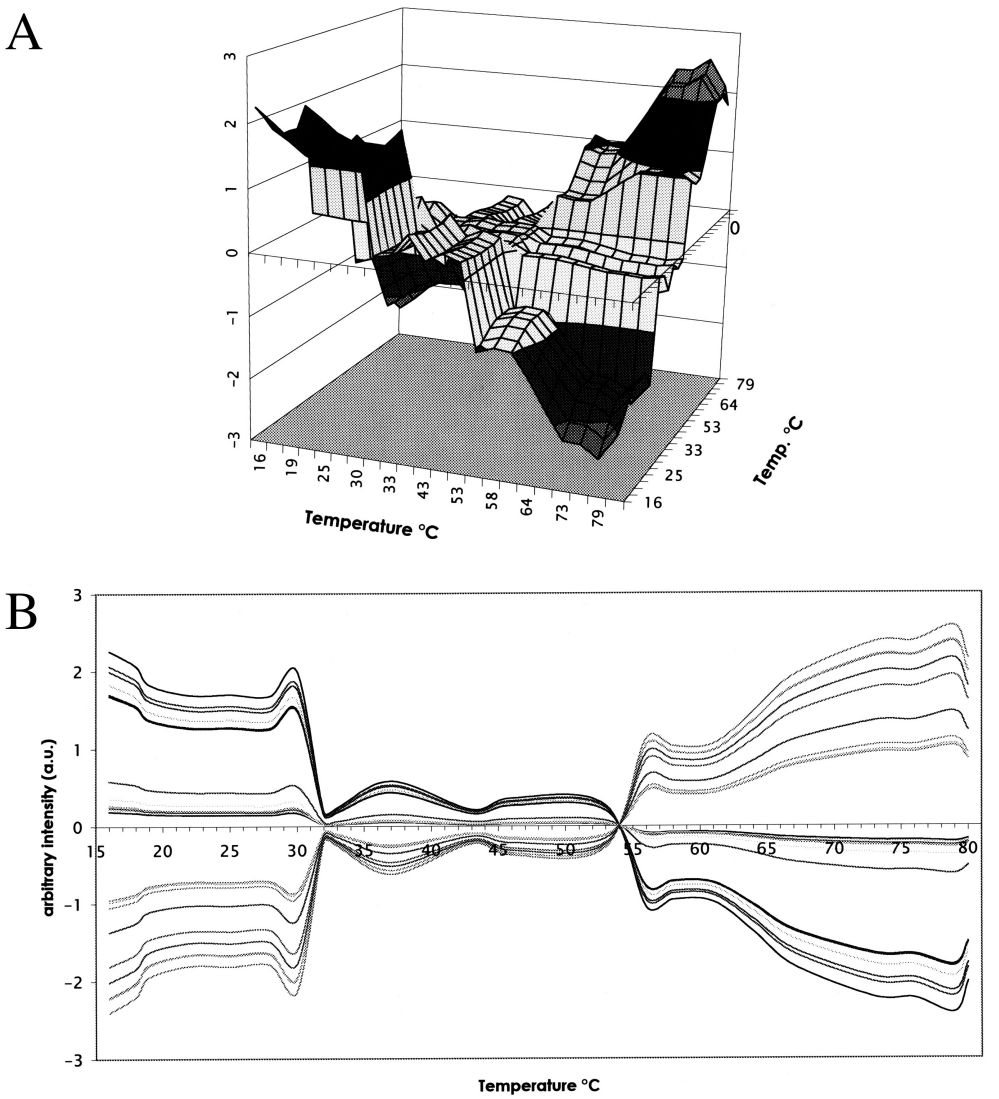

Fig. 16. (A) A synchronous spectrum of the sample–sample correlation caoculated from the spectra shown in Fig. 14. (B) The slice spectra of the three-demensional representation shown in Fig. 16(A). (Reproduced from Ref. 59 with permission. Copyright (2000) American Chemical Societies).

phasize the spectral variations through the whole region. Therefore, evidence for the phase transition of oleic acid based on the intensity change in the band at 6917 cm^{-1} becomes less significant compared with the evidence from the rest of the spectra. In other words, information about the dissociation of the dimer is suppressed since only the band at 6917 cm^{-1} is strongly related to the monomer. Instead, in Figs. 15 and 16 the changes in the physical properties of oleic acid become important. The correlation patterns in these figures are concerned mostly with the spectral variations in the 7600–6950 cm^{-1} region where all the spectral dynamics is governed by the temperature-dependent density change and changes in other physical properties of the sample. Accordingly, Šašič et al.[59] concluded that the three kinds of liquid structures of oleic acid for the temperature ranges of 15–32 , 32–55 and 55–80 °C are distinguished based upon the spectral changes that reflect the variations in the physical properties of oleic acid.

The successful application of the newly proposed method for investigating the concentration dynamic is specially notable. This method can be easily understood and applied to the systems where a process similar to the monomerization of dimers takes place. All the advantages and limitations of the generalized 2D methodology are preserved in the sample–sample correlation. Therefore, the method is not restricted on this kind of perturbation – the same approach is valid for monitoring concentration changes of species with time, pressure etc.

7. Future Aspects

Generalized 2D correlation spectroscopy has opened new era in spectral analysis. Application of 2D correlation analysis in various branches of optical spectroscopy and in various fields of science and engineering have expanded greatly since

the introduction of the generalized 2D correlation concept. These enormous progress in 2D correlation spectroscopy has been strongly supported by the availability of new hardware for efficient and precise spectral experiments and software for the easy but reliable computation of 2D spectra.

For further development of 2D correlation spectroscopy there are several important issues. One is to explore a new possibility of 2D correlation spectroscopy. Recently proposed sample–sample correlation spectroscopy is one such example. Another is the development of quantitative interpretation methods for 2D spectra. Yet another is comparison with other spectral analysis methods such as cheometrics.[60]

Recently, the concept of 2D correlation spectroscopy has become wider and wider, and besides generalized 2D correlation spectroscopy, several 2D correlation spectroscopies were born. For example, a variety of multidimensional off-resonant Raman and resonant optical and IR techniques have been developed.[20,63] Thus, comparison among a variety of 2D correlation spectroscopies may provide new or deeper insight into 2D methods. Of course, there is always the possibility of a new generation of 2D spectroscopy.

References

1 W. P. Aue, E. Bartholdi, and R. R. Ernst, *J. Chem. Phys.*, **64**, 2229 (1976).

2 K. Nagayama, A. Kumar, K. Wüthrich, and R. R. Ernst, *J. Magn. Reson.*, **40**, 321 (1980).

3 A. Bax, "Two Dimensional Nuclear Magnetic Resonance in Liquids," Reidel, Boston (1982).

4 R. R. Ernst, G. Bodenhausen, and A. Wakaun, "Principles of Nuclear Magnetic Resonance in One and Two Dimensions," Oxford University Press, Oxford (1987).

5 I. Noda, *Bull. Am. Phys. Soc.*, **31**, 520 (1986).

6 I. Noda, *J. Am. Chem. Soc.*, **111**, 8116 (1989).

7 I. Noda, *Appl. Spectrosc.*, **44**, 550 (1990).

8 I. Noda, *Chemtracts-Macromol. Chem.*, **1**, 89 (1990).

9 C. Marcott, A. E. Dowrey, and I. Noda, *Anal. Chem.*, **66**, 1065A (1994).

10 I. Noda, A. E. Dowrey, and C. Marcott in "Modern Polymer Spectroscopy," ed by G. Zerbi, Wiley-VCH, Weinheim (1999), p.1.

11 I. Noda, A. E. Dowrey, and C. Marcott, *Appl. Spectrosc.*, **47**, 1317 (1993).

12 I. Noda, A. E. Dowrey, and C. Marcott, *Appl. Spectrosc.*, **42**, 203 (1988).

13 R. A. Palmer, C. J. Manning, J. L. Chao, I. Noda, A. E. Dowrey, and C. Marcott, *Appl. Spectrosc.*, **45**, 12 (1991).

14 C. Marcott, A. E. Dowrey, and I. Noda, *Appl. Spectrosc.*, **47**, 1324 (1993).

15 V. G. Gregoriou, J. L. Chao, H. Toriumi, and R. A. Palmer, *Chem. Phys. Lett.*, **179**, 491.

16 S. V. Shilov, S. Okretic, H. W. Siesler, and M. A. Scarnecki, *Appl. Spectrosc. Rev.*, **31**, 125 (1996).

17 M. Sonoyama, K. Shoda, G. Katagiri, and H. Ishida, *Appl. Spectrosc.*, **50**, 377 (1996).

18 I. Noda, *Appl. Spectrosc.*, **47**, 1329 (1993).

19 I. Noda, A. E. Dowrey, C. Marcott, Y. Ozaki, and G. M. Story, *Appl. Spectrosc.*, In press.

20 Y. Ozaki and I. Noda, Eds. "Two-Dimensional Correlation Spectroscopy, AIP Conference Proceedings," American Institute of Physics, New York (2000), Vol. 503, p. 3.

21 I. Noda, Ref. 20, p.3.

22 I. Noda, Y. Liu, and Y. Ozaki, *J. Phys. Chem.*, **100**, 8674 (1996).

23 M. A. Czarnecki, P. Wu, H. W. Siesler, *Chem. Phys. Lett.*, **283**, 326 (1998).

24 C. P. Schultz, H. Fabian, and H. H. Mantsch, *Biospectrosc.*, **4**, 519 (1998).

25 A. Matsushita, Y. Ren, K. Matsukawa, H. Inoue, Y. Minami, I. Noda, and Y. Ozaki, *Vib. Spectrosc.*, In press.

26 Y. Ren, A. Matsushita, K. Matsukawa, H. Inoue, Y. Minami, I. Noda, and Y. Ozaki, *Vib. Spectrosc.*, In press.

27 Y. Jung, B. Czarnik-Matusewicz, and Y. Ozaki, *J. Phys. Chem. B*, **104**, 7812 (2000).

28 I. Noda, "Dynamic Infrared Dichroism and Two-Dimensional Correlation Spectroscopy," Doctoral Thesis, The University of Tokyo, 1997.

29 I. Noda, *Appl. Spectrosc.*, In press.

30 Y. Ozaki, Y. Liu, and I. Noda, *Macromolecules*, **30**, 2391 (1997).

31 E. J. Hannan, "Multiple Time Series," John Wiley & Sons, New York (1970).

32 D. R. Brillinger, "Time Series Data Analysis and Theory," Holt, Rinehart and Winston, New York (1975).

33 L. J. Frasinski, K. Codling, and P. A. Hatherly, *Science*, **246**, 1029 (1989).

34 C. Marcott, I. Noda, and A. Dowrey, *Anal. Chim. Acta*, **250**, 131 (1991).

35 F. B. Barton II, D. S. Himmelsbach, J. H. Duckworth, and M. J. Smith, *Appl. Spectrosc.*, **46**, 420 (1992).

36 J.-R. Burie, *Appl. Spectrosc.*, **50**, 861 (1996).

37 I. Noda, Ref. 20, p. 201.

38 I. Noda, Y. Liu, Y. Ozaki, and M. A. Czarnecki, *J. Phys. Chem.*, **99**, 3068 (1995).

39 Y. Liu, Y. Ozaki, and I. Noda, *J. Phys. Chem.*, **100**, 7326 (1996).

40 M. Muller, R. Buchet, and U. P. Fringeli, *J. Phys. Chem.*, **100**, 10810 (1996).

41 A. Nabet and M. Pezolet, *Appl. Spectrosc.*, **51**, 466 (1997).

42 I. Noda, G. M. Story, A. E. Dowrey, R. C. Reeder, and C. Marcott, *Macromol. Symp.*, **119**, 1 (1997).

43 M. Osawa, *Bull. Chem. Soc. Jpn.*, **70**, 2861 (1997).

44 N. L. Sefara, N. P. Magtoto, and H. H. Richardson, *Appl. Spectrosc.*, **51**, 536 (1997).

45 Y. Wang, K. Murayama, Y. Myojo, R. Tsenkova, N. Hayashi, and Y. Ozaki, *J. Phys. Chem. B*, **34**, 6655 (1998).

46 M. A. Czarnecki, H. Maeda, Y. Ozaki, M. Suzuki, and M. Iwahashi, *Appl. Spectrosc.*, **52**, 994 (1998).

47 N. P. Magtoto, N. L. Sefara, and H. H. Richardson, *Appl. Spectrosc.*, **53**, 178 (1999).

48 L. Smeller and K. Heremans, *Vibrat. Spectrosc.*, **19**, 375 (1999).

49 P. Pancoska, J. Kubelka, and T. Keiderling, *Appl. Spectrosc.*, **53**, 655 (1999).

50 Y. Ren, M. Shinoyama, T. Ninomiya, K. Matsukawa, H. Inoue, I. Noda, and Y. Ozaki, *J. Phys. Chem. B*, **103**, 6475 (1999).

51 B. Czarnik-Matusewicz, K. Murayama, R. Tsenkova, and Y. Ozaki, *Appl. Spectrosc.*, **12**, 1582 (1999).

52 Y. Liu, Y.-R. Chen, and Y. Ozaki, *Appl. Spectrosc.*, **4**, 587 (2000).

53 Y. Nagasaki, T. Yoshihara, and Y. Ozaki, *J. Phys. Chem. B*,

104, 2846 (2000).
54 H. Okumura, M. Sonoyama, K. Okuno, Y. Nagasawa, and H. Ishida, in Ref. 20, p. 232.
55 Y. Wu, B. Czarnik-Matusewicz, K. Murayama, and Y. Ozaki, *J. Phys. Chem. B*, **104**, 5840 (2000).
56 B. Czarnik-Matusewicz, K. Murayama, Y. Wu, and Y. Ozaki, *J. Phys. Chem. B*, **104**, 7803 (2000).
57 K. Nakashima, S. Yasuda, I. Noda, and Y. Ozaki, *J. Phys. Chem. B*, in press.
58 S. Šašič, A. Muszynski, and Y. Ozaki, *J. Phys. Chem. B*, **104**, 6380 (2000).
59 S. Šašič, A. Muszynski, and Y. Ozaki, *J. Phys. Chem. B*, **104**, 6388 (2000).
60 S. Šašič, A. Muszynski, and Y. Ozaki, submitted for publication.
61 M. Iwahashi, Y. Yamaguchi, T. Kato, T. Horiuchi, I. Sakurai, and M. Suzuki, *J. Phys. Chem.*, **95**, 445 (1991).
62 M. Iwahashi, N. Hachiya, Y. Hayashi, H. Matsuzawa, M. Suzaki, Y. Fujimoto, and Y. Ozaki, *J. Phys. Chem.*, **97**, 3129 (1993).
63 S. Mukamel, "Principles of Nonlinear Optical Spectroscopy," Oxford University Press, New York (1995).

Yukihiro Ozaki was born in Sakai, Osaka Japan. He graduated from Osaka University in 1973 with B.S degree in chemistry. He also obtained his M.S (1975) and Ph.D. (1978) in chemistry from Osaka University. After he spent for two years and a half at National Research Council, Canada as a research associate, he joined the Jikei University School of Medicine in Tokyo in 1981. In 1989 he moved to Kwansei Gakuin University at Nishinomiya as an associate professor of Chemistry Department. Currently, he holds a position of Professor in the Department of Chemistry, School of Science. His research program has been concerned with applications of infrared, Raman, and near-infrared (NIR) spectroscopy, especially their applications to functional materials such as organic thin films, liquid crystals, polymers, and biological materials. He research interests have also involved spectral analysis methods such as two-dimensional correlation spectroscopy and chemometrics. He received the 1998 Tomas Hirschfeld Award at Pittsburgh Conference from the International Committee of Near-Infrared Spectroscopy for his contribution in the development of spectral analysis in NlR spectroscopy. He has also been selected as the recipient of the 2001 EAS Award for the Achievements in NIR Spectroscopy.

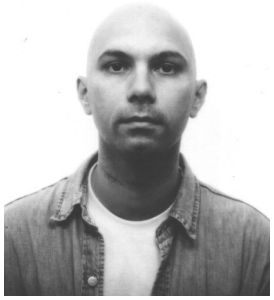

Slobodan Šašič was born in Vrsac (Yugoslavia) 1967. He obtained his B.S. (1992), MSc (1995) and Ph.D (1998) from University of Belgrade, Faculty of Physical Chemistry. The object of his Ph.D thesis was application of chemometrics for resolving different complex Raman spectral systems. Since 1.9.1999 he is postdoctoral fellow in Prof. Y. Ozaki group. The main targets of his research in Japan are theory and application of 2D spectroscopy, application of calibration based methods and self-modeling curve resolution methods in qualitative and quantitative analyses of biological materials and polymers.

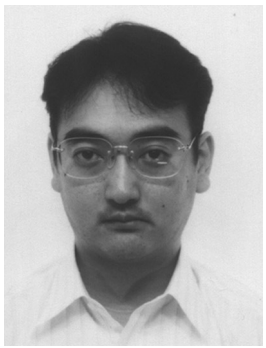

Takeyuki Tanaka was born in Osaka, Japan. He was graduated with B.S. degree in chemistry from Osaka University in 1992. He also received his M.Phil. (1994) and Ph.D. (1998) in physical chemistry from Osaka University. His research interest is in the field of vibrational spectroscopies, especially, vibrational circular dichroism spectroscopy, which he studied at the Institue for Protein Research, Osaka University. His recently interest study is surface enhanced Raman scattering. In addition, he is active in the area of simulation for infrared, vibrational circular dichroism, Raman, and UV-Visible spectra and chemical shift of NMR by *ab inito* molecular orbital methods, which he studied at Osaka National Research Institute, Agency of Industrial Science and Technology. He is currently a Research Fellow of Kwansei-Gakuin University. After he worked at Kwansei-Gakuin University as a research fellow, he joined Kobe University as an assistant professor.

Isao Noda was born in Tokyo, Japan. He came to the United States in 1969 and was graduated from Columbia University in the City of New York in 1974 with B.S. degree in chemical engineering. He also received his M.S. in bioengineering (1976) and M.Phil. (1978) and Ph.D. (1979) in chemical engineering from Columbia. In 1997 he received D.Sc. degree in Chemistry from the University of Tokyo. His research interest is in the area of polymer physics, especially spectroscopic and rheological characterization of polymers. He is also active in the area of solution, surface and colloid chemistry of polymers. He is currently a Research Fellow of the Procter and Gamble Company.